

Probability density function and Reynolds-stress modeling of near-wall turbulent flows

Thomas D. Dreeben and Stephen B. Pope

Sibley School of Mechanical and Aerospace Engineering, Cornell University, Ithaca, New York 14853

(Received 28 December 1995; accepted 4 September 1996)

Probability density function (pdf) methods are extended to include modeling of wall-bounded turbulent flows. A pdf near-wall model is developed in which the generalized Langevin model is combined with an exact model for viscous transport. Then the method of elliptic relaxation is used to incorporate the wall effects without the use of wall functions or damping functions. Information about the proximity of the wall is provided only in the boundary conditions so that the model can be implemented without *ad hoc* assumptions about the geometry of the flow. A Reynolds-stress closure is derived from this pdf model, and its predictions are compared with DNS and experimental results for fully developed turbulent channel flow. © 1997 American Institute of Physics. [S1070-6631(97)02201-0]

I. INTRODUCTION

Turbulent flows are especially difficult to model in the near-wall region, because the flow there is strongly inhomogeneous and anisotropic. Most Reynolds-stress models work well only for quasi-homogeneous flows.¹⁻⁴ Many efforts to incorporate the effects of the wall in turbulence models involve the use of wall functions.⁵⁻⁷ With this approach, boundary conditions which are consistent with the logarithmic law of the wall are imposed just beyond the viscous sublayer, so that the difficult modeling very close to the wall is avoided. Wall functions have also been used with the probability density function (pdf) method in the calculation of recirculating flows.⁸

The use of damping functions⁹ allows models to incorporate the no-slip condition and to capture the behavior in the viscous sublayer. In Reynolds-stress closures, damping functions are used to connect a quasi-homogeneous model far from the wall with asymptotically correct Reynolds-stress behavior close to the wall. Several models of this sort are reviewed in Ref. 10.

A common requirement with these approaches is that information about the proximity of the wall needs to be provided in the flow domain itself, either in the governing equations, or (in the case of wall functions) in the boundary conditions, or both. This necessity is considered to be a weakness, because the methods require some *a priori* information about the flow in order to be implemented. Such a requirement undermines the capability of these methods to extend to flows with complex geometries.

Recent developments in near-wall modeling have successfully eliminated the explicit dependence on the distance from the wall of the governing equations, both with¹¹ and without¹²⁻¹⁵ the use of damping functions. Those models which have no damping functions use the method of elliptic relaxation.¹² Here the terms for the effects of fluctuating pressure are modeled using an elliptic equation. This necessitates boundary conditions on the pressure terms as well as the velocities; these additional boundary conditions are chosen to bring about accurate near-wall behavior of the Reynolds stresses.

In this work we take the first step in extending the pdf method so that it includes the accurate modeling of wall-bounded turbulent flows. We formulate a pdf model which uses elliptic relaxation to allow the no-slip condition to be imposed at the wall without requiring information about the proximity of the wall anywhere else in the flow domain. Feasibility of the model is assessed by deriving the corresponding Reynolds-stress closure, and comparing the Reynolds-stress statistics with available DNS data for fully developed channel flow. In Section II, we use a standard Taylor series analysis to bring out the important features of near-wall flows to be represented by the model. Section III introduces the pdf formulation by showing the appropriate pdf evolution equation for the Navier–Stokes equations; this equation is to be closed with the model. Section IV gives the full development of the model. There we derive the pdf closure, the corresponding Reynolds-stress closure, and wall boundary conditions on the Reynolds stresses. In Section V we discuss the capability of the model to reproduce the behavior of fully developed channel flow. Realizability is discussed in Section VI.

II. NEAR-WALL REYNOLDS STRESSES

Here we use a standard Taylor series analysis¹⁶ to examine the near-wall Reynolds-stress equations and their solutions. Results of this analysis are important in the construction of the model. We split the velocity and pressure into the familiar Reynolds decomposition:

$$U_i = \langle U_i \rangle + u_i, \quad (1)$$

$$\mathcal{P} = \langle \mathcal{P} \rangle + p. \quad (2)$$

For

$$\frac{\tilde{D}(\cdot)}{Dt} = \frac{\partial(\cdot)}{\partial t} + \langle U_k \rangle \frac{\partial(\cdot)}{\partial x_k}, \quad (3)$$

the exact Reynolds-stress equation is

$$\frac{\tilde{D}\langle u_i u_j \rangle}{Dt} = T_{(v)ij} + T_{(t)ij} + P_{ij} + \phi_{ij} - \epsilon_{ij}, \quad (4)$$

TABLE I. Near-wall Reynolds-stress terms as functions of y to first order.

i,j	$T_{(v)ij}$	ϕ_{ij}	ϵ_{ij}
1,1	$2\nu\langle b_1^2 \rangle$	$O(y)$	$2\nu\langle b_1^2 \rangle$
2,2	$12\nu\langle c_2^2 \rangle y^2$	$-2\langle c_2 b_p \rangle y^2$	$8\nu\langle c_2^2 \rangle y^2$
3,3	$2\nu\langle b_3^2 \rangle$	$O(y)$	$2\nu\langle b_3^2 \rangle$
1,2	$6\nu\langle b_1 c_2 \rangle y$	$-\langle b_1 b_p \rangle y$	$4\nu\langle b_1 c_2 \rangle y$

where the terms on the right-hand side represent viscous transport, turbulent transport, production, velocity-pressure gradient correlations, and dissipation, respectively. It is important to note that ϕ_{ij} includes both pressure transport and redistribution. Though the analysis is valid for any wall bounded flow, coordinates are arranged here to accommodate statistically one-dimensional flow, such as fully developed channel flow: u, x_1 are aligned with the mean flow, $v, y = x_2$ are wall-normal, and w, x_3 are in the spanwise direction. To describe the near-wall behavior, the fluctuating velocities and pressure are expanded in a Taylor series about the wall¹⁶ where $a_i, b_i, c_i, \dots, i = 1, 2, 3$ and a_p, b_p, c_p, \dots are random functions of x_1, x_3 , and time,

$$u = a_1 + b_1 y + c_1 y^2 + \dots, \quad (5)$$

$$v = a_2 + b_2 y + c_2 y^2 + \dots, \quad (6)$$

$$w = a_3 + b_3 y + c_3 y^2 + \dots, \quad (7)$$

$$p = a_p + b_p y + c_p y^2 + \dots. \quad (8)$$

By imposing the boundary conditions of no slip and impermeability, and the governing equations for conservation of mass and momentum, we find the following results for the Reynolds stresses: First, to leading order, the scaling of each Reynolds stress with distance from the wall is

$$\langle u^2 \rangle \sim y^2, \quad (9)$$

$$\langle v^2 \rangle \sim y^4, \quad (10)$$

$$\langle w^2 \rangle \sim y^2, \quad (11)$$

$$\langle uv \rangle \sim y^3. \quad (12)$$

Second, the dominant balance of Reynolds-stress terms near the wall is

$$T_{(v)ij} + \phi_{ij} - \epsilon_{ij} = 0. \quad (13)$$

The scaling with y of these dominant terms is given for each Reynolds-stress equation in Table I. And third, Taylor series expansions for $k = \frac{1}{2}\langle u_i u_i \rangle$ and $\epsilon = \frac{1}{2}\epsilon_{ii}$ can be used to show that to leading order, the unknown terms ϕ_{ij} and ϵ_{ij} can be modeled exactly in terms of known quantities, $\langle u_i u_j \rangle, k$, and ϵ :

$$\epsilon_{11} \sim \frac{\epsilon}{k} \langle u^2 \rangle, \quad (14)$$

$$\phi_{22} \sim -2 \frac{\epsilon}{k} \langle v^2 \rangle, \quad (15)$$

$$\epsilon_{22} \sim 4 \frac{\epsilon}{k} \langle v^2 \rangle, \quad (16)$$

$$\epsilon_{33} \sim \frac{\epsilon}{k} \langle w^2 \rangle, \quad (17)$$

$$\phi_{12} \sim - \frac{\epsilon}{k} \langle uv \rangle, \quad (18)$$

$$\epsilon_{12} \sim 2 \frac{\epsilon}{k} \langle uv \rangle. \quad (19)$$

Using these, we express the near-wall Reynolds-stress equations to first order in closed form:

$$\nu \frac{\partial^2 \langle u^2 \rangle}{\partial y^2} - \frac{\epsilon}{k} \langle u^2 \rangle = 0, \quad (20)$$

$$\nu \frac{\partial^2 \langle v^2 \rangle}{\partial y^2} - 6 \frac{\epsilon}{k} \langle v^2 \rangle = 0, \quad (21)$$

$$\nu \frac{\partial^2 \langle w^2 \rangle}{\partial y^2} - \frac{\epsilon}{k} \langle w^2 \rangle = 0, \quad (22)$$

$$\nu \frac{\partial^2 \langle uv \rangle}{\partial y^2} - 3 \frac{\epsilon}{k} \langle uv \rangle = 0. \quad (23)$$

These equations embody the important balance of physical processes close to the wall: They are to be used for guidance in the construction of the pdf near-wall model.

The above results bring out the strong anisotropy and inhomogeneity which need to be addressed in the modeling of near-wall flows. The anisotropy is clear from the terms in Table I. The dominant processes are of order (1) at the wall in the (1,1) and (3,3) directions, but they vanish in the directions which have a normal component; the turbulence becomes two-component as the wall is approached. Summing the diagonal terms of the Reynolds-stress equations in Table I shows that the contributions to the dissipation of kinetic energy near the wall are only important in the (1,1) and (3,3) directions. The inhomogeneity in the wall normal direction appears in Eqs. (20)–(23) where the viscous transport dominates the balance of every Reynolds-stress component. Elliptic relaxation¹³ has been shown to model these near-wall effects well in Reynolds-stress closures; we hope to capture these effects by incorporating elliptic relaxation in the pdf approach.

III. PDF EVOLUTION EQUATION WITH MOLECULAR VISCOSITY

Let $f(\mathbf{V}; \mathbf{x}, t)$ be the Eulerian pdf of velocity at a given location. The evolution equation for the Eulerian pdf can be expressed in two ways:¹⁷

$$\begin{aligned} \frac{\partial f}{\partial t} + V_i \frac{\partial f}{\partial x_i} &= \frac{1}{\rho} \frac{\partial \langle \mathcal{P} \rangle}{\partial x_i} \frac{\partial f}{\partial V_i} \\ &+ \frac{\partial}{\partial V_i} \left[f \left\langle \frac{1}{\rho} \frac{\partial p}{\partial x_i} - \nu \frac{\partial^2 U_i}{\partial x_j \partial x_j} \right| \mathbf{U}(\mathbf{x}, t) = \mathbf{V} \right] \end{aligned} \quad (24)$$

or

$$\begin{aligned} \frac{\partial f}{\partial t} + V_i \frac{\partial f}{\partial x_i} = & \nu \frac{\partial^2 f}{\partial x_j \partial x_j} + \frac{1}{\rho} \frac{\partial \langle \mathcal{P} \rangle}{\partial x_i} \frac{\partial f}{\partial V_i} \\ & - \frac{\partial^2}{\partial V_i \partial V_j} \left[f \left\langle \nu \frac{\partial U_i}{\partial x_k} \frac{\partial U_j}{\partial x_k} \right| \mathbf{U}(\mathbf{x}, t) = \mathbf{V} \right] \\ & + \frac{\partial}{\partial V_i} \left[f \left\langle \frac{1}{\rho} \frac{\partial p}{\partial x_i} \right| \mathbf{U}(\mathbf{x}, t) = \mathbf{V} \right]. \end{aligned} \quad (25)$$

For modeling in which viscosity is important, we use Eq. (25), because the first term on its right-hand side represents viscous diffusion exactly. That term leads to the important viscous terms in the near-wall balances of Eqs. (20)–(23). Only the terms on the first line of Eq. (25) are in closed form, so an appropriate pdf model must provide a closure approximation for the remaining terms.

IV. PDF NEAR-WALL MODEL

The model to be developed here provides both a pdf and a Reynolds-stress closure. Here, we construct both versions in five stages. First, particle equations which represent the Navier–Stokes equations exactly are derived in a way which leads to exact representation of viscous transport. Second, the generalized Langevin model is used to close the unknown terms of the particle equations. The important parameters in this model are specified using Durbin’s elliptic relaxation. Third, we derive the resulting pdf model by closing Eq. (25) with a modeled pdf evolution equation, and by providing an equation for dissipation. Fourth, we formulate the Reynolds-stress version of the model by deriving velocity moment equations, and by adding a model for turbulent transport. Fifth, Reynolds-stress boundary conditions are imposed and the near-wall behavior is compared with the correct near-wall behavior described previously. This model development is guided by two main priorities:

- (1) Far from the wall, the model approaches the familiar isotropization of production (IP) model.^{1,2}
- (2) Close to the wall, the dominant balance of terms as represented in Eq. (13) is modeled as accurately as possible.

A. Exact particle equations

Consider an ensemble of particles moving through the Eulerian velocity field $\mathbf{U}(\mathbf{x}, t)$ with particle position $\mathcal{X}(t)$ and velocity $\mathcal{U}(t)$. For $\mathbf{U}(\mathbf{x}, t)$ governed by the Navier–Stokes equations, we define the particle velocity as the Eulerian fluid velocity evaluated at the particle position:

$$\mathcal{U}(t) = \mathbf{U}[\mathcal{X}(t), t]. \quad (26)$$

We seek equations to govern the position and velocity of these particles in which the viscous stress is modeled exactly.

Previous pdf formulations have used fluid particles. With this approach, the change in particle position $d\mathcal{X}$ over an infinitesimal time interval dt is determined by the local fluid velocity:^{17,18}

$$d\mathcal{X}_i = \mathcal{U}_i dt. \quad (27)$$

By this definition, fluid particles are convected through the velocity field; consequently these models represent convec-

tive transport exactly. But fluid particles are inadequate for capturing viscous transport, because any pdf evolution equation which follows from Eq. (27) [such as Eq. (24)] must exclude the important viscous term $\nu(\partial^2 f / \partial x_i \partial x_i)$, which appears in Eq. (25) (see for example Ref. 18). In an effort to capture the effects of both convective and viscous transport, we consider stochastic particles which undergo both convective and molecular motion. So we combine Eq. (27) with the classical model for Brownian motion¹⁹ in which the change in position of a molecule is governed by a symmetric probability distribution. To characterize this random motion, we use the isotropic Wiener process \mathbf{W} in which increments have a normal distribution with zero mean, and

$$dW_i dW_j = dt \delta_{ij}. \quad (28)$$

Then increments of particle position are given by

$$d\mathcal{X}_i = \mathcal{U}_i dt + \sqrt{2\nu} dW_i, \quad (29)$$

where $\sqrt{2\nu}$ is chosen to ensure that the momentum carried by these particles diffuses in physical space with coefficient ν . So the particles carry momentum with them in the same way that molecules do, and with identical statistics. This particle motion leads to the viscous transport term in Eq. (25), and hence to the viscous terms in the near-wall balances of Eqs. (20)–(23).

We now find the corresponding increment of particle velocity $d\mathcal{U}$. For an arbitrary change in position $d\mathcal{X}$ over the small time interval dt , we have

$$d\mathcal{U}_i = \frac{\partial U_i}{\partial t} dt + \frac{\partial U_i}{\partial x_j} d\mathcal{X}_j + \frac{1}{2} \frac{\partial^2 U_i}{\partial x_j \partial x_k} d\mathcal{X}_j d\mathcal{X}_k + \dots \quad (30)$$

We substitute Eq. (29) into Eq. (30) and retain the terms up to order dt :

$$d\mathcal{U}_i = \frac{\partial U_i}{\partial t} dt + \frac{\partial U_i}{\partial x_j} (\mathcal{U}_j dt + \sqrt{2\nu} dW_j) + \nu \frac{\partial^2 U_i}{\partial x_j \partial x_j} dt. \quad (31)$$

Note that the Wiener process in Eq. (31) is identical to the one which appears in the equation for position, Eq. (29). Next we rewrite the first two terms on the right hand side of Eq. (31), using Eq. (26) and the Navier–Stokes equations:

$$d\mathcal{U}_i = -\frac{1}{\rho} \frac{\partial \mathcal{P}}{\partial x_i} dt + 2\nu \frac{\partial^2 U_i}{\partial x_j \partial x_j} dt + \sqrt{2\nu} \frac{\partial U_i}{\partial x_j} dW_j. \quad (32)$$

Equation (32) describes the change in velocity of a particle whose position evolves by Eq. (29) through a velocity field which is governed by the Navier–Stokes equations.

B. Generalized Langevin model with elliptic relaxation

We now construct model particle equations to approximate Eqs. (29) and (32). Throughout this section we denote modeled quantities and pdfs with an asterisk superscript to distinguish them from their exact counterparts. Let $f^*(\mathbf{V}; \mathbf{x}, t)$ be the modeled Eulerian pdf; this is the pdf of velocity at a given location \mathbf{x} and time t . Then mean velocities are defined as

$$\langle \mathbf{U}_i^*(\mathbf{x}, t) \rangle = \int V_i f^* d\mathbf{V}, \quad (33)$$

with the integral taken over all of velocity space. For modeling in a context in which Eulerian velocities are unknown, Eq. (32) is divided into closed and unclosed terms with the Reynolds decomposition:

$$d\mathcal{U}_i = -\frac{1}{\rho} \frac{\partial \langle \mathcal{P} \rangle}{\partial x_i} dt + 2\nu \frac{\partial^2 \langle U_i \rangle}{\partial x_j \partial x_j} dt + \sqrt{2\nu} \frac{\partial \langle U_i \rangle}{\partial x_j} dW_j - \frac{1}{\rho} \frac{\partial p}{\partial x_i} dt + 2\nu \frac{\partial^2 u_i}{\partial x_j \partial x_j} dt + \sqrt{2\nu} \frac{\partial u_i}{\partial x_j} dW_j. \quad (34)$$

Then we define the motion of modeled particles with position $\mathcal{X}^*(t)$ and velocity $\mathcal{U}^*(t)$. Increments of position are given by Eq. (29), and increments in velocity are defined by using the generalized Langevin model to replace the unclosed terms of Eq. (34):

$$d\mathcal{X}_i^* = \mathcal{U}_i^* dt + \sqrt{2\nu} dW_i, \quad (35)$$

$$d\mathcal{U}_i^* = -\frac{1}{\rho} \frac{\partial \langle \mathcal{P}^* \rangle}{\partial x_i} dt + 2\nu \frac{\partial^2 \langle U_i^* \rangle}{\partial x_j \partial x_j} dt + \sqrt{2\nu} \frac{\partial \langle U_i^* \rangle}{\partial x_j} dW_j + G_{ij} (\mathcal{U}_j^* - \langle U_j^* \rangle) dt + \sqrt{C_0 \epsilon^*} dW_i'. \quad (36)$$

Here, \mathbf{W}' is another isotropic Wiener process, independent of \mathbf{W} , and ϵ^* is the modeled mean dissipation rate. The generalized Langevin model has parameters G_{ij} and C_0 , which jointly provide a model for the fluctuating pressure gradients and the fluctuating velocities.

To complete the generalized Langevin model, we specify the parameters G_{ij} and C_0 , using Durbin's method of elliptic relaxation.^{12,13} In this approach the terms which involve fluctuating pressure gradients are modeled with an elliptic equation, by analogy with the fact that the pressure is governed by the Poisson equation. This represents the non-local effect of the wall on the Reynolds stresses through the fluctuating pressure terms. We introduce a tensor ϕ_{ij} to characterize the non-local effect of fluctuating pressure, and set

$$G_{ij} = \frac{\epsilon^*}{k^*} \frac{\phi_{ij} - \frac{\epsilon^*}{2} \delta_{ij}}{k^*}, \quad (37)$$

$$C_0 = \frac{-2\phi_{ij} \langle u_i^* u_j^* \rangle}{3k^* \epsilon^*}, \quad (38)$$

where k^* is the modeled turbulent kinetic energy. While C_0 is often constant in pdf models, it is chosen here to insure that ϕ_{ij} be purely redistributive (Durbin²⁸).

To define ϕ_{ij} we first specify time and length scales. Following Durbin, we take the maximum of the turbulent scales and the Kolmogorov scales:

$$T = \max \left[\frac{k^*}{\epsilon^*}, C_T \sqrt{\frac{\nu}{\epsilon^*}} \right], \quad (39)$$

$$L = C_L \max \left[\frac{k^*{}^{3/2}}{\epsilon^*}, C_\eta \left(\frac{\nu^3}{\epsilon^*} \right)^{1/4} \right], \quad (40)$$

where C_T , C_L , and C_η are model constants. Then we specify the non-local term ϕ_{ij} with the following elliptic-relaxation equation:

$$\phi_{ij} - L\nabla^2(L\phi_{ij}) = \frac{(1-C_1)k^*}{2T} \delta_{ij} + k^* H_{ijkl} \frac{\partial \langle U_k^* \rangle}{\partial x_l}, \quad (41)$$

where

$$H_{ijkl} = \left(C_2 A_v + \frac{1}{3} \gamma_5 \right) \delta_{ik} \delta_{jl} - \frac{1}{3} \gamma_5 \delta_{il} \delta_{jk} + \gamma_5 b_{ik} \delta_{jl} - \gamma_5 b_{il} \delta_{jk}, \quad (42)$$

$$A_v = \min \left[1.0, C_v \frac{\det \langle u_i u_j \rangle}{\left(\frac{2}{3} k \right)^3} \right], \quad (43)$$

and

$$b_{ij} = \frac{\langle u_i u_j \rangle}{\langle u_k u_k \rangle} - \frac{1}{3} \delta_{ij} \quad (44)$$

is the Reynolds-stress anisotropy tensor. The right-hand side of Eq. (41) is the family of stochastic Lagrangian versions of a modified IP model²⁰ with parameter γ_5 , and with IP model constants C_1 and C_2 . Far from the wall, ϕ_{ij} dominates the Laplacian term on the left hand side of Eq. (41), so the current model approaches the IP model. Close to the wall, the Laplacian term becomes important and brings out the non-local response of the pressure fluctuations to the boundary conditions.

The Laplacian term of Eq. (41) and the modification of the IP model which is embodied in Eq. (43) warrant further explanation. They are both efforts to improve the behavior of the model in the inertial sublayer where the mean velocity varies logarithmically with y , a common difficulty with elliptic relaxation models.^{13,21} The present model decreases the sensitivity of the Reynolds stresses to non-local effects in the log layer based an idea which appears in Ref. 22. The elliptic expression

$$L\nabla^2(L\phi_{ij}) \quad (45)$$

appears in Eq. (41), rather than the more commonly used expression

$$L^2\nabla^2\phi_{ij}. \quad (46)$$

Under the constant-stress assumptions of the logarithmic layer, we have

$$\phi_{ij} \sim \frac{1}{y}, \quad (47)$$

$$L \sim y, \quad (48)$$

so the elliptic term (45) vanishes whereas the elliptic term (46) does not. As a result of the term (45), Reynolds stresses in the log layer are determined primarily by local turbulent quantities.

The modification of the IP model involves incorporating the term A_v in Eq. (42). The behavior of the logarithmic profile is sensitive to ϕ_{ij} , which in turn is most sensitive to

the IP model source term in question. Durbin has argued¹² that in a $k - \epsilon$ type closure, the turbulent viscosity scales with the wall normal turbulent intensity $\langle v^2 \rangle^*$ rather than with k^* , and hence is suppressed close to the wall. By analogy, this pdf model captures the logarithmic layer more accurately when the IP source term is similarly suppressed near the wall. The term A_v is an invariant which behaves like $\langle v^2 \rangle^*/k^*$ close to the wall (for an appropriately chosen constant C_v). Far from the wall, we have $A_v = 1.0$, and the source term is identical to that of the standard IP model. This modification improves the behavior of the mean velocity profile in the log layer, with the IP model constant $C_2 = 0.63$. The fact the C_2 is close to its original value of $C_2 = 0.6$ preserves the ability of the current model to characterize a sudden distortion of initially isotropic turbulence, as the original IP model does.¹

The complete model particle formulation is given by Eqs. (35)–(44). The values of the constants are given below in Eq. (63).

C. Closure at the pdf level

Here we close Eq. (25), based on the model of the previous section. The asterisk superscript notation is dropped, with the understanding that all physical variables and pdfs are modeled quantities. We define two model pdfs: Let $f_L(\mathbf{V}, \mathbf{x}; t)$ be the Lagrangian pdf; this is the joint pdf of a particle's position and velocity. The pdf of particle position is

$$f_x(\mathbf{x}; t) = \int f_L(\mathbf{V}, \mathbf{x}; t) d\mathbf{V}. \quad (49)$$

Then the Eulerian pdf is the Lagrangian pdf of the particle velocity, conditioned on the particle's position:

$$f(\mathbf{V}; \mathbf{x}, t) = \frac{f_L(\mathbf{V}, \mathbf{x}; t)}{f_x(\mathbf{x}; t)}. \quad (50)$$

Starting from the particle equations (35) and (36), we derive an evolution equation for each of these pdfs sequentially to arrive at the Eulerian pdf equation.

The Lagrangian pdf evolution equation follows from taking Eqs. (35) and (36) to be a six dimensional diffusion process. Then by the methods in Ref. 23, the Lagrangian pdf evolves by

$$\begin{aligned} \frac{\partial f_L}{\partial t} + V_i \frac{\partial f_L}{\partial x_i} = & \nu \frac{\partial^2 f_L}{\partial x_i \partial x_i} + \frac{\partial f_L}{\partial V_i} \frac{1}{\rho} \frac{\partial \langle \mathcal{P} \rangle}{\partial x_i} - \frac{\partial}{\partial V_i} [G_{ij}(V_j \\ & - \langle U_j \rangle) f_L] + 2\nu \frac{\partial \langle U_j \rangle}{\partial x_i} \frac{\partial^2 f_L}{\partial x_i \partial V_j} \\ & + \nu \frac{\partial \langle U_i \rangle}{\partial x_k} \frac{\partial \langle U_j \rangle}{\partial x_k} \frac{\partial^2 f_L}{\partial V_i \partial V_j} + \frac{1}{2} C_0 \epsilon \frac{\partial^2 f_L}{\partial V_i \partial V_i}. \end{aligned} \quad (51)$$

The evolution for the pdf of position is obtained by integrating Eq. (51) over velocity space:

$$\frac{\partial f_x}{\partial t} + \frac{\partial [\langle U_i \rangle f_x]}{\partial x_i} = \nu \frac{\partial^2 f_x}{\partial x_i \partial x_i}. \quad (52)$$

For modeling an incompressible turbulent flow, we impose

$$\frac{\partial \langle U_i \rangle}{\partial x_i} = 0, \quad (53)$$

plus initial and boundary conditions on $\mathcal{X}^*(t)$ so that $f_x(\mathbf{x}; t)$ is constant at $t=0$ and on the boundaries of the flow domain. These conditions ensure that

$$f_x(\mathbf{x}; t) = \text{constant} \quad (54)$$

is the only solution to Eq. (52). Then we find the Eulerian pdf equation by dividing Eq. (51) by f_x :

$$\begin{aligned} \frac{\partial f}{\partial t} + V_i \frac{\partial f}{\partial x_i} = & \nu \frac{\partial^2 f}{\partial x_i \partial x_i} + \frac{\partial f}{\partial V_i} \frac{1}{\rho} \frac{\partial \langle \mathcal{P} \rangle}{\partial x_i} - \frac{\partial}{\partial V_i} [G_{ij}(V_j \\ & - \langle U_j \rangle) f] + 2\nu \frac{\partial \langle U_j \rangle}{\partial x_i} \frac{\partial^2 f}{\partial x_i \partial V_j} \\ & + \nu \frac{\partial \langle U_i \rangle}{\partial x_k} \frac{\partial \langle U_j \rangle}{\partial x_k} \frac{\partial^2 f}{\partial V_i \partial V_j} + \frac{1}{2} C_0 \epsilon \frac{\partial^2 f}{\partial V_i \partial V_i}. \end{aligned} \quad (55)$$

The random term in Eq. (35) has led to the important viscous term $\nu \partial^2 f / \partial x_i \partial x_i$ in the modeled Eulerian pdf equation [first term on the right hand side of Eq. (55)]. The model provides a closure to Eq. (25) by setting

$$\begin{aligned} \frac{\partial}{\partial V_i} \left[f \left\langle \frac{1}{\rho} \frac{\partial p}{\partial x_i} \right| \mathbf{U} = \mathbf{V} \right] - \frac{\partial^2}{\partial V_i \partial V_k} \left[f \left\langle \nu \frac{\partial U_k}{\partial x_i} \frac{\partial U_l}{\partial x_i} \right| \mathbf{U} = \mathbf{V} \right] \\ = - \frac{\partial}{\partial V_i} [G_{ij}(V_j - \langle U_j \rangle) f] + 2\nu \frac{\partial \langle U_j \rangle}{\partial x_i} \frac{\partial^2 f}{\partial x_i \partial V_j} \\ + \nu \frac{\partial \langle U_i \rangle}{\partial x_k} \frac{\partial \langle U_j \rangle}{\partial x_k} \frac{\partial^2 f}{\partial V_i \partial V_j} + \frac{1}{2} C_0 \epsilon \frac{\partial^2 f}{\partial V_i \partial V_i}. \end{aligned} \quad (56)$$

To complete the closure at the pdf level, we use Durbin's modeled equation for the dissipation:

$$\begin{aligned} \frac{\tilde{D}\epsilon}{Dt} = \frac{\partial}{\partial x_i} \left[\left(\nu + \frac{C_\mu}{\sigma_\epsilon} \langle u_i u_j \rangle T \right) \frac{\partial \epsilon}{\partial x_j} \right] + C_{\epsilon 1} \left(1 + a_1 \frac{P}{\epsilon} \right) \frac{P}{T} \\ - C_{\epsilon 2} \frac{\epsilon}{T}, \end{aligned} \quad (57)$$

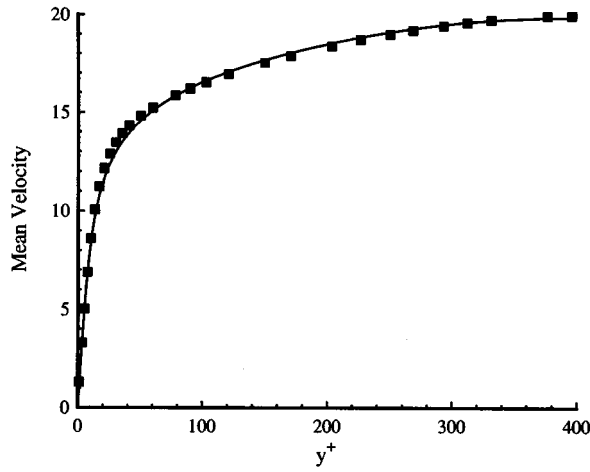
where

$$P = - \langle u_i u_j \rangle \frac{\partial \langle U_i \rangle}{\partial x_j} \quad (58)$$

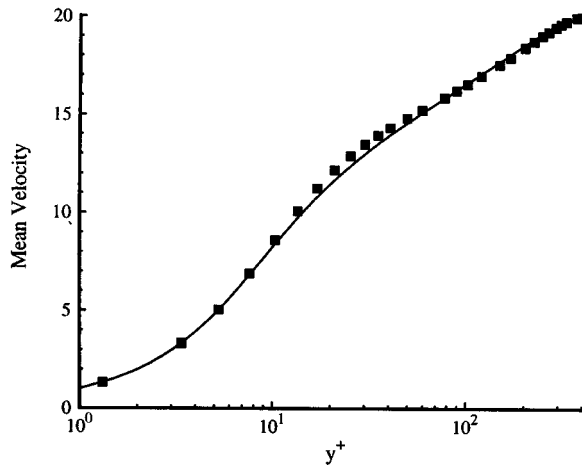
is the production of turbulent kinetic energy. The model constants in this equation, given in Eq. (63), have nearly identical values (only a_1 differs slightly) to those which appear in Ref. 13.

D. Closure at the Reynolds-stress level

Every pdf model has a corresponding Reynolds-stress closure.²⁰ We derive the Reynolds-stress version of the current model by taking first and second moments of the pdf equation. The mean velocity equation is derived by multiplying Eq. (55) by V_i and integrating over velocity space. This gives the familiar Reynolds equations exactly:



(a)



(b)

FIG. 1. Mean velocity for fully developed channel flow: comparison of model (line) with DNS data (symbols).

$$\frac{\tilde{D}\langle U_j \rangle}{Dt} + \frac{\partial}{\partial x_i} \langle u_i u_j \rangle = -\frac{1}{\rho} \frac{\partial \langle \mathcal{P} \rangle}{\partial x_j} + \nu \frac{\partial^2 \langle U_j \rangle}{\partial x_i \partial x_i}. \quad (59)$$

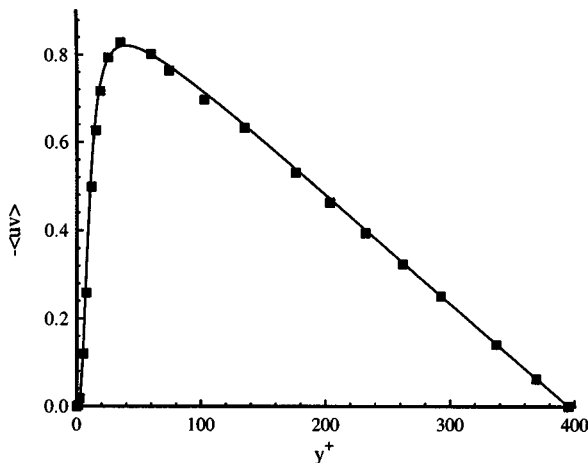


FIG. 2. Reynolds shear stress for fully developed channel flow: comparison of model (line) with DNS data (symbols).

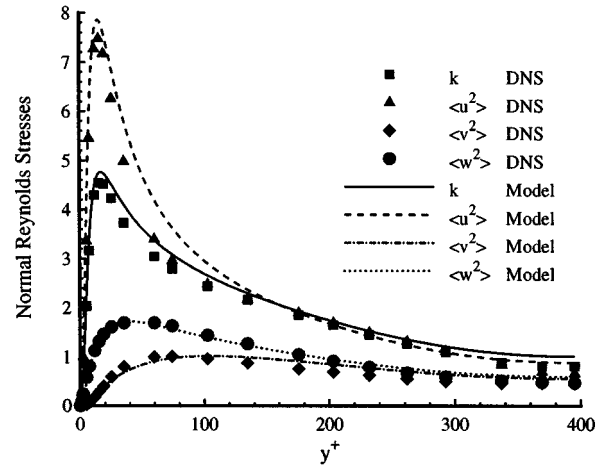


FIG. 3. Normal Reynolds stresses for fully developed channel flow: comparison of model (line) with DNS data (symbols).

To derive the Reynolds-stress equation, we multiply Eq. (55) by the quantity $(V_i - \langle U_i \rangle)(V_j - \langle U_j \rangle)$ and integrate over velocity space to give

$$\begin{aligned} \frac{\tilde{D}\langle u_i u_j \rangle}{Dt} = & \nu \frac{\partial^2 \langle u_i u_j \rangle}{\partial x_k \partial x_k} - \frac{\partial \langle u_i u_j u_k \rangle}{\partial x_k} \\ & - \left(\langle u_i u_k \rangle \frac{\partial \langle U_j \rangle}{\partial x_k} + \langle u_j u_k \rangle \frac{\partial \langle U_i \rangle}{\partial x_k} \right) \\ & + G_{ik} \langle u_k u_j \rangle + G_{jk} \langle u_k u_i \rangle + C_0 \epsilon \delta_{ij}. \end{aligned} \quad (60)$$

By comparing Eq. (60) with (4), we see that the generalized Langevin terms model combined effects of fluctuating velocity-pressure-gradient correlations and dissipation:

$$\phi_{ij} - \epsilon_{ij} = G_{ik} \langle u_k u_j \rangle + G_{jk} \langle u_k u_i \rangle + C_0 \epsilon \delta_{ij}. \quad (61)$$

At the Reynolds-stress level, we also need a model for the turbulent transport term $T_{(t)ij} = \partial \langle u_i u_j u_k \rangle / \partial x_k$. We follow Durbin¹³ and use the Daly and Harlow²⁴ gradient-diffusion model:

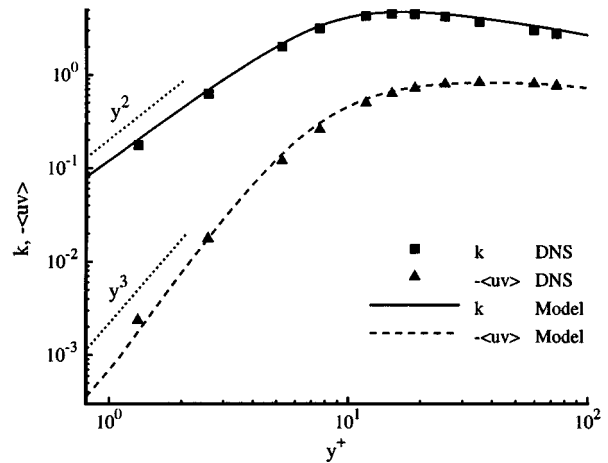


FIG. 4. Near-wall scaling of kinetic energy and Reynolds shear stress for fully developed channel flow: comparison of model (line) with DNS data (symbols).

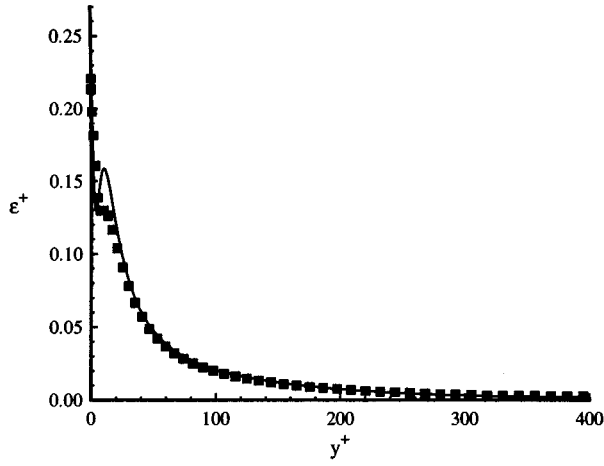


FIG. 5. Dissipation of turbulent kinetic energy for fully developed channel flow: comparison of model (line) with DNS data (symbols).

$$T_{(t)ij} = \frac{\partial}{\partial x_k} \left(\frac{C_\mu}{\sigma_k} \langle u_k u_l \rangle T \frac{\partial \langle u_i u_j \rangle}{\partial x_l} \right). \quad (62)$$

The model constant values in this term, given in Eq. (63), are identical to those in Ref. 13. The complete Reynolds-stress closure is specified by Eqs. (37)–(44), (53), (57)–(60), and (62). Model constants are

$$\begin{aligned} C_1 &= 1.8; \quad C_2 = 0.63; \quad C_v = 1.4; \quad C_\mu = 0.23; \quad \sigma_k = 1.2; \\ \gamma_5 &= 0.1; \quad \sigma_\epsilon = 1.65; \quad C_{\epsilon 1} = 1.44; \quad C_{\epsilon 2} = 1.9; \\ a_1 &= 0.09; \quad C_T = 6.0; \quad C_L = 0.134; \quad C_\eta = 72.0. \end{aligned} \quad (63)$$

E. Boundary conditions and near-wall behavior

At the wall, we impose the no-slip condition on the mean and fluctuating velocities, and we set \wp_{ij} as follows:

$$\langle U_i \rangle = 0, \quad (64)$$

$$\langle u_i u_j \rangle = 0, \quad (65)$$

$$n_i \frac{\partial k}{\partial x_i} = 0, \quad (66)$$

$$\wp_{ij} = -17.2 \frac{\epsilon^2}{v \frac{\partial \langle U_m \rangle}{\partial x_k} \frac{\partial \langle U_m \rangle}{\partial x_l} n_k n_l} n_i n_j, \quad (67)$$

where \mathbf{n} is the wall normal. Because the only non-zero component of \wp_{ij} at the wall is in the normal direction, the model can be implemented in more complicated geometries without additional assumptions about the direction of the mean flow. The condition on \wp_{ij} controls the near-wall suppression of Reynolds shear stress through its appearance in Eq. (71); hence it also controls the position of the velocity profile. It embodies a weak Reynolds number dependence, expressed in terms of quantities at the wall. This enables the model to reproduce the observed velocity profiles over different Reynolds numbers.

The near-wall behavior follows from the form of the model and from the boundary conditions. For the exact physical case, we found the near-wall behavior in Section II

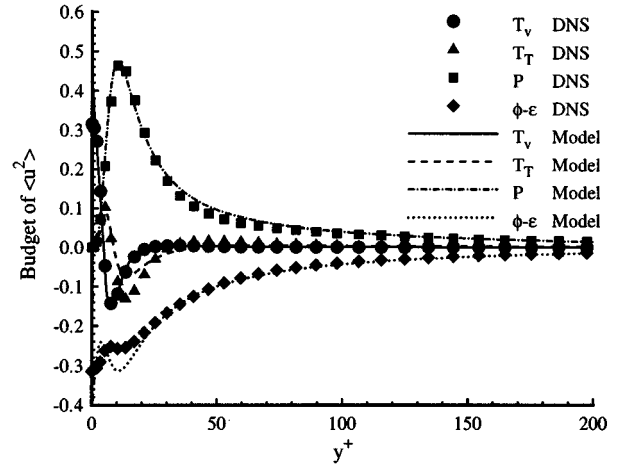


FIG. 6. Budget of $\langle u^2 \rangle$ for fully developed channel flow: comparison of model (line) with DNS data (symbols).

by expanding the fluctuating velocities in a Taylor series about the wall. That method does not work with a turbulence model, because the model says nothing about fluctuating velocities; only moments of the velocity. Instead, we derive modeled near-wall counterparts of Eqs. (20)–(23) by expanding each Reynolds stress in a Taylor series about the wall, imposing the boundary conditions of Eqs. (64)–(67), and the Reynolds-stress equations of Eq. (60). Close to the wall, the model equations become

$$v \frac{\partial^2 \langle u^2 \rangle}{\partial y^2} - \frac{\epsilon}{k} \langle u^2 \rangle = 0, \quad (68)$$

$$v \frac{\partial^2 \langle v^2 \rangle}{\partial y^2} + \frac{4}{3} \wp_{22} \frac{\epsilon}{k} \langle v^2 \rangle = O(y), \quad (69)$$

$$v \frac{\partial^2 \langle w^2 \rangle}{\partial y^2} - \frac{\epsilon}{k} \langle w^2 \rangle = 0, \quad (70)$$

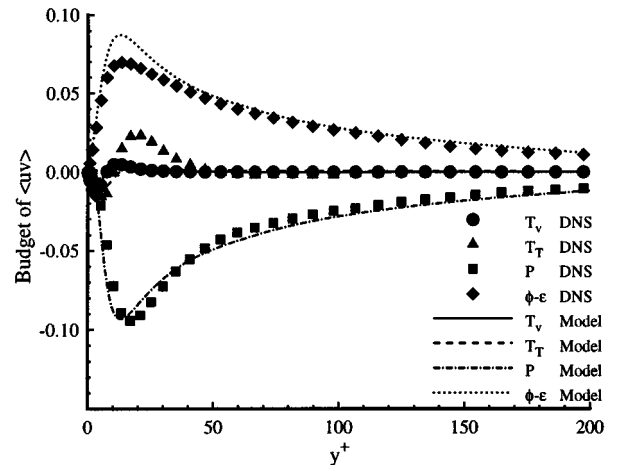


FIG. 7. Budget of $\langle uv \rangle$ for fully developed channel flow: comparison of model (line) with DNS data (symbols).

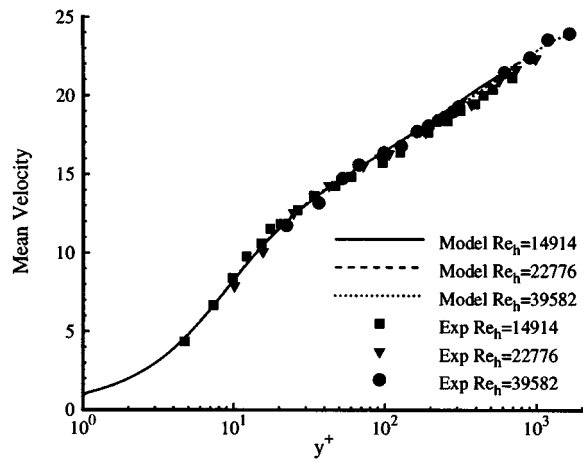


FIG. 8. Mean velocity for fully developed channel flow: comparison of model (line) with data of Wei and Willmarth (symbols) at different Reynolds numbers.

$$\nu \frac{\partial^2 \langle uv \rangle}{\partial y^2} + \frac{\phi_{22} - \epsilon}{k} \langle uv \rangle = O(y), \quad (71)$$

with solutions

$$\langle u^2 \rangle \sim y^2, \quad (72)$$

$$\langle v^2 \rangle \sim y^3, \quad (73)$$

$$\langle w^2 \rangle \sim y^2, \quad (74)$$

$$\langle uv \rangle \sim y^3. \quad (75)$$

It is clear from comparing Eqs. (68)–(71) with Eqs. (20)–(23) that the model reproduces the dominant balance of transport with dissipation in the near-wall Reynolds stresses exactly in the tangential directions. To leading order, this aspect of the model captures the near-wall anisotropy. Near-wall inhomogeneity is also captured with the appearance of the exact viscous transport terms on the left-hand side of Eqs. (68)–(71). Comparison of Eqs. (72)–(75) with Eqs. (9)–(12) shows that all Reynolds stresses scale correctly

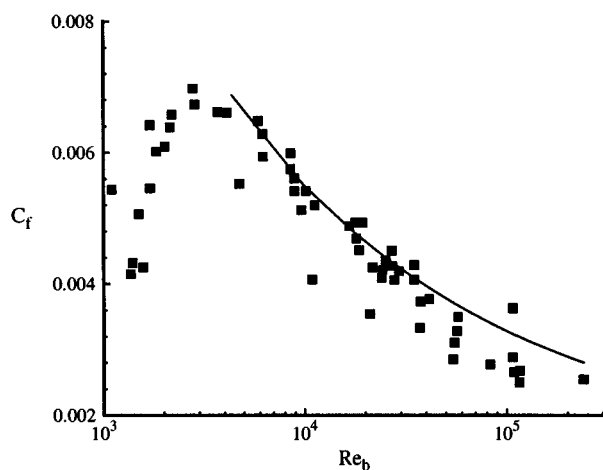


FIG. 9. Friction coefficient as a function of Reynolds number for fully developed channel flow: comparison of model (line) with data compiled by Dean.

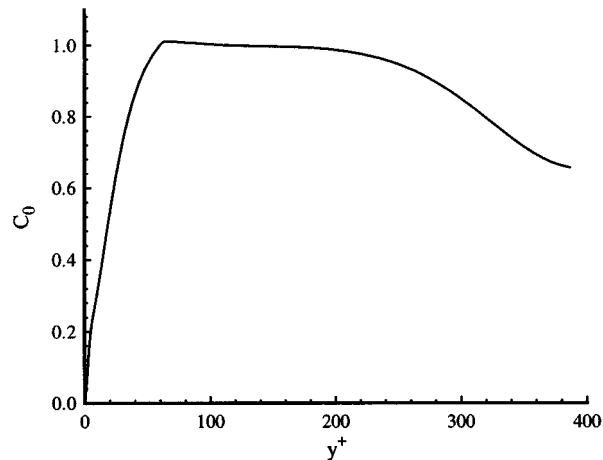


FIG. 10. A test of realizability: C_0 should always be positive.

with y near the wall, except for $\langle v^2 \rangle$, which approaches zero as y^3 rather than at the correct rate of y^4 . But the important processes (those of order 1) are the portions of viscous transport and dissipation which occur only in the (1,1), and (3,3) directions near the wall; this analysis shows that the model represents those balances correctly. So before considering any calculations, we know that the model can characterize important aspects of near-wall flows.

V. FULLY DEVELOPED CHANNEL FLOW

The model is tested for fully developed channel flow with $Re_\tau = 395$, based on the friction velocity and the channel half-width. The Reynolds-stress equations are discretized on a 150 cell grid, and solved with Newton's method using a fully implicit scheme. Model predictions of velocity, Reynolds stresses, and dissipation are shown in Figs. 1 through 5, together with DNS data of Mansour.²⁸

Model predictions of Reynolds-stress budgets of $\langle u^2 \rangle$ and $\langle uv \rangle$ up to $y^+ = 200$ are shown in Figs. 6 and 7. All velocities shown are normalized with the friction velocity and plotted against the distance from the wall in wall units. It should be understood that the current model provides an expression for the difference of pressure correlation and dissipation terms in Eq. (61), but not for each term separately. Consequently, the quantity $\phi_{ij} - \epsilon_{ij}$ is shown in the budgets.

Generally adequate agreement is achieved with the mean velocity profile and with the Reynolds stresses. This includes the logarithmic behavior of the mean velocity above $y^+ = 40$. The analysis of the near-wall behavior in Section IV E gives good agreement with the near-wall scaling of k and $\langle uv \rangle$ in Fig. 4.

The most significant discrepancies in the budgets coincide with inaccuracies in the model for turbulent transport. The overprediction of transport at $y^+ = 10$ in Fig. 6 corresponds to the underprediction of $\phi_{11} - \epsilon_{11}$ there, and to the underprediction of the dissipation close to the wall in Fig. 5. In the budget of Reynolds shear stress, there is also an underprediction of turbulent transport, together with an overprediction of $\phi_{12} - \epsilon_{12}$ at $y^+ = 15$. It is hoped that these de-

partures can be improved by the full pdf version of the model in which the turbulent transport is represented in the governing equations exactly.

Model velocity profiles and friction coefficient over varying Reynolds numbers are shown in Figs. 8 and 9. For each case, the chosen number of grid cells is proportional to the Reynolds number. The velocity profiles are compared to the experimental channel flow data of Wei and Willmarth²⁵ at Reynolds numbers $Re_h = 14914, 22776, \text{ and } 39582$, with Re_h based on the mean velocity at the channel halfplane and on the channel halfwidth. Using the model, these correspond to $Re_\tau = 695, 1012, \text{ and } 1658$ respectively. (Wei and Willmarth report $Re_\tau = 1655$ in the highest Reynolds number case, by expressing the location of the halfplane in wall units.) Model results for the friction coefficient are compared with the experimental data compiled by Dean.²⁶ For half-plane mean velocity $\langle U \rangle_h$, the friction coefficient $C_f = \tau_w / \frac{1}{2}\rho \langle U \rangle_h^2$, is plotted against the Reynolds number Re_b , based on the bulk mean velocity and the full channel width. Plausible agreement is achieved with the model in both cases.

VI. MODEL REALIZABILITY

By its construction, a well-posed pdf model is guaranteed to satisfy realizability.¹⁷ Well-posedness at the pdf level and realizability at the Reynolds-stress level go hand in hand, and they depend on whether the coefficient C_0 of Eqs. (36) and (38) is non-negative.²⁷ It can be shown from Eq. (38) that

$$C_0 \rightarrow \frac{2}{3} \left(C_1 + C_2 \frac{P}{\epsilon} - 1 \right) \quad (76)$$

far from the wall [where the elliptic term of Eq. (41) becomes small] and that

$$C_0 \rightarrow 0 \quad (77)$$

as y approaches the wall. Figure 10 shows that the model gives realizable results in the case of channel flow. But there is no analytical guarantee that C_0 remains non-negative everywhere. Should the need arise to impose realizability with more complex flows, a simple modification to the model can be used: Let

$$\beta = 1 + \max \left(\frac{-2\varphi_{ij} \langle u_i u_j \rangle}{3k\epsilon}, 0 \right). \quad (78)$$

Then we replace Eqs. (37) and (38) with

$$G_{ij} = \frac{\varphi_{ij} - \frac{\beta\epsilon}{2} \delta_{ij}}{k}, \quad (79)$$

$$C_0 = \frac{2}{3} \left(\beta - 1 - \frac{\varphi_{ij} \langle u_i u_j \rangle}{k\epsilon} \right). \quad (80)$$

These specifications guarantee realizable solutions to the Reynolds-stress closure, and that $\frac{1}{2} \langle u_i u_i \rangle$ continues to satisfy the equation for turbulent kinetic energy

$$\frac{Dk}{Dt} = \nu \frac{\partial^2 k}{\partial x_i \partial x_i} + \frac{\partial}{\partial x_j} \left(\frac{C_\mu}{\sigma_k} \langle u_i u_j \rangle T \frac{\partial k}{\partial x_j} \right) + P - \epsilon. \quad (81)$$

Figure 10 shows values of C_0 which are significantly lower than the values previously used in pdf models, such as Ref. 18 in which $C_0 = 2.1$. This is a consequence of choosing the source terms of Eq. (41) to match the IP model; for this case Eq. (76) predicts that $C_0 = 0.95$ far from the wall where production and dissipation are comparable.

VII. CONCLUSION

The objective of the current model is to extend pdf methods so that they accurately resolve the statistics of turbulent flows in the near-wall region. This is achieved with two innovations: First, a random term is introduced in the equation for particle position, Eq. (29). This necessitates a new approach to the development of the physical particle evolution equations, and provides an exact model for viscous transport which is a dominant process near the wall. Second, Durbin's elliptic relaxation is used in the generalized Langevin model to incorporate the non-local effect of the wall on the Reynolds stresses. With these techniques, the near-wall Reynolds-stress equations are well approximated, and the strong anisotropy and inhomogeneity of the flow close to the wall is modeled to reasonable accuracy. The predictions for fully developed channel flow show that the model is a viable extension of pdf methods to handle wall bounded flows. For future work, the model will be solved as a pdf model using a Monte Carlo method, and it will be tested with more complex wall bounded turbulent flows.

ACKNOWLEDGMENTS

We wish to thank Paul Durbin and Alfred Schatz for useful discussions and support of this work. In particular, we thank Paul Durbin for suggesting the use of Eq. (38) in the model. The work was supported by AFOSR Award No. F49620-93-1-0316.

¹B. E. Launder, G. J. Reece, and W. Rodi, "Progress in the development of a Reynolds-stress turbulence closure," *J. Fluid Mech.* **68**, 537 (1975).

²D. Naot, A. Shavit, and M. Wolfshtein, "Interactions between components of the turbulent velocity correlation tensor," *Isr. J. Technol.* **8**, 259 (1970).

³T. S. Shih and J. L. Lumley, "Modeling of pressure correlation terms in Reynolds stress and scalar flux equations," Technical Report No. FDA-85-3, Cornell University, Ithaca, NY, March 1985.

⁴C. G. Speziale, S. Sarkar, and T. B. Gatski, "Modelling the pressure-strain correlation of turbulence: An invariant dynamical systems approach," *J. Fluid Mech.* **209**, 245 (1991).

⁵B. E. Launder and D. B. Spalding, "The numerical computation of turbulent flows," *Comp. Methods Appl. Mech. Eng.* **3**, 269 (1974).

⁶A. K. Singhal and D. B. Spalding, "Predictions of two-dimensional boundary layers with the aid of the $k-\epsilon$ model of turbulence," *Comp. Methods Appl. Mech. Eng.* **25**, 365 (1981).

⁷W. Rodi, *Turbulence models and their application in hydraulics—a state of the art review* (International Association for Hydraulic Research, Delft, The Netherlands, 1980).

⁸M. S. Anand, S. B. Pope, and H. C. Mongia, "A pdf method for turbulent recirculating flows," in *Turbulent Reactive Flows*, Lecture Notes in Engineering (Springer-Verlag, Berlin, 1989), pp. 672–693.

⁹E. R. Van Driest, "On turbulent flow near a wall," *J. Aeronaut. Sci.* **23**, 1007 (1956).

¹⁰R. M. C. So, Y. G. Lai, and H. S. Zhang, "Second-order near-wall turbulence closures: A review," *Am. Inst. Aeronaut. Astroaut. J.* **29**, 1819 (1991).

¹¹T. J. Craft and B. E. Launder, "Improvements in near-wall Reynolds-Stress modelling for complex flow geometries," in *Tenth Symposium on*

- Turbulent Shear Flows*, 1995 (Pennsylvania State University, University Park, PA, 1995).
- ¹²P. A. Durbin, "Near-wall turbulence closure modeling without damping functions," *Theo. Comp. Fluid Dyn.* **3**, 1 (1991).
- ¹³P. A. Durbin, "A Reynolds-stress model for near-wall turbulence," *J. Fluid Mech.* **249**, 465 (1993).
- ¹⁴D. Laurence, P.A. Durbin, and A. O. Demuren, "Modelling near-wall effects in second moment closures by elliptic relaxation," in *Tenth Symposium on Turbulent Shear Flows*, 1995 (Pennsylvania State University, University Park, PA, 1995).
- ¹⁵A. O. Demuren and S. Sarkar, "Systematic study of Reynolds-stress closure models in the computations of plane channel flows," Technical Report No. 92-19, ICASE, April 1992.
- ¹⁶N. N. Mansour, J. Kim, and P. Moin, "Reynolds-stress and dissipation-rate budgets in a turbulent channel flow," *J. Fluid Mech.* **194**, 15 (1988).
- ¹⁷S. B. Pope, "Pdf methods for turbulent reactive flows," *Prog. Energy Combust. Sci.* **11**, 119 (1985).
- ¹⁸D. C. Haworth and S. B. Pope, "A generalized Langevin model for turbulent flows," *Phys. Fluids A* **29**, 387 (1986).
- ¹⁹A. Einstein, *Investigations on the Theory of the Brownian Movement*, translation by A. D. Cowper, edited by R. Furth (Methuen, London, 1926).
- ²⁰S. B. Pope, "On the relationship between stochastic Lagrangian models of turbulence and second moment closures," *Phys. Fluids* **6**, 973 (1993).
- ²¹T. D. Dreeben and S. B. Pope, "Pdf and Reynolds stress modeling of near-wall turbulent flows," in *Tenth Symposium on Turbulent Shear Flows*, 1995 (Pennsylvania State University, University Park, PA, 1995).
- ²²D. Laurence, P. A. Durbin, and A. O. Demuren, "Modelling near-wall effects in second moment closures by elliptic relaxation," in *Proceedings of the Summer Program, Center for Turbulence Research*, 1994 (Stanford University, Stanford, CA, 1994).
- ²³N. Wax, *Noise and Stochastic Processes* (Dover, New York, 1954).
- ²⁴B. J. Daly and F. H. Harlow, "Transport equations of turbulence," *Phys. Fluids* **13**, 2634 (1970).
- ²⁵T. Wei and W. W. Willmarth, "Reynolds-number effects on the structure of a turbulent channel flow," *J. Fluid Mech.* **204**, 57 (1989).
- ²⁶R. B. Dean, "Reynolds number dependence of skin friction and other bulk flow variables in two-dimensional rectangular duct flow," *J. Fluids Eng.* **100**, 215 (1978).
- ²⁷P. A. Durbin and C. G. Speziale, "Realizability of second moment closure via stochastic analysis," Technical Report, Center for Turbulence Research, Stanford, CA, September 1993.
- ²⁸P. A. Durbin (private communication).